Reaction dynamics of metal/oxide catalysts: Methanol oxidation at vanadium oxide films on Rh(1 1 1) from UHV to 10^{-2} mbar

Bernhard von Boehn [a], Christopher Penschke [b,1], Xiaoke Li [b], Joachim Paier [b,*], Joachim Sauer [b], Jon-Olaf Krisponeit [c,d], Jan Ingo Flege [c,d,e], Jens Falta [c,d], Helder Marchetto [f], Torsten Franz [f], Gerhard Lilienkamp [g], Ronald Imbihl [a,*]

[a] Institut für Physikalische Chemie und Elektrochemie, Leibniz Universität Hannover, Callinstrasse 3A, 30167 Hannover, Germany
[b] Institut für Chemie, Humboldt-Universität zu Berlin, 10099 Berlin, Germany
[c] University of Bremen, Institute of Solid State Physics, 28359 Bremen, Germany
[d] MAPEX Center for Materials and Processes, University of Bremen, 28359 Bremen, Germany
[e] Brandenburgische Technische Universität Cottbus-Senftenberg, Fachgebiet Angewandte Physik und Halbleiterspektroskopie, 03046 Cottbus, Germany
[f] Elmitec Elektronenmikroskopie GmbH, 38678 Clausthal-Zellerfeld, Germany
[g] Institute of Energy Research and Physical Technologies, Technische Universität Clausthal, 38678 Clausthal-Zellerfeld, Germany

ARTICLE INFO

ABSTRACT

Recent advances in in situ microscopy allow to follow the reaction dynamics during a catalytic surface reaction from ultra-high vacuum to 0.1 mbar, thus bridging a large part of the pressure gap. Submonolayer vanadium oxide films on Rh(1 1 1) have been studied during catalytic methanol oxidation in situ with spatially resolving imaging techniques. At 10^{-6}–10^{-4} mbar VO_x condenses into macroscopic circular islands that exhibit a substructure, consisting of a reduced island core and an oxidized outer ring. This substructure arises due to an oxygen gradient inside the VO_x islands, which results in different coexisting 2D-phases of VO_x on Rh(1 1 1). This substructure is also responsible for a "breathing-like" oscillatory expansion and contraction that the islands undergo under stationary conditions. Using density functional theory, the 2D-phase diagram of VO_x on Rh(1 1 1) has been computed. The oscillatory behavior can be understood as a periodic phase transition between two 2D phases of VO_x. With a newly developed near ambient pressure – low-energy electron microscope, it was shown that VO_x islands disintegrate at 10^{-2} mbar, resulting in turbulent dynamics.

© 2020 Elsevier Inc. All rights reserved.

1. Introduction

Catalytic surfaces restructure under reaction conditions with the extent ranging from atomic-scale reconstructions to real morphological changes and chemical transformations [1–3]. As a consequence of dynamic processes governing the composition and structure of a catalyst in operation, a pressure gap exists between surface science studies conducted in UHV and "real catalysis", operating typically in a pressure range from ≈1–100 bar [4,5]. A key challenge in heterogeneous catalysis is therefore the development of in situ and operando techniques, which allow monitoring a catalyst in its active state.

The reaction-induced restructuring processes, often associated with an activation of the catalyst, are well documented for metal surfaces, but comparatively little is known about the dynamics of oxide catalysts under reaction conditions. As a model system for supported oxide catalysts we investigate submonolayer vanadium oxide films on a Rh(1 1 1) surface. Vanadium oxide catalysts are among the most important catalysts in chemical industry, finding application in many partial oxidation reactions, e.g. formaldehyde production from methanol in the formox process [6,7], sulfuric acid production and the selective catalytic reduction (SCR) process in environmental chemistry [8]. The geometric and electronic structure of pure and supported vanadium oxides, their reactivity, and the influence of the support material have been the subject of numerous studies [9–16].

The high catalytic efficiency of V-oxides can be attributed to the ability of vanadium to easily change the oxidation state between V^{3+}, V^{4+}, and V^{5+} under reaction conditions [8,9,14,17]. In industrial applications V-oxide is usually deposited on an oxidic support

material such as SiO_2, Al_2O_3, ZrO_2, TiO_2 or Ce_2O_3, to name just the most commonly used ones [18]. The choice of the support material was shown to have a strong influence on the catalytic properties of V-oxide [15]. There is general agreement that V-oxide in its catalytically most active form is highly dispersed, either in the form of isolated V_xO_y-clusters or as a monomolecular 2D-film. In the mechanistic description of partial oxidation reactions most scientists prefer the two-step model developed by Mars and van Krevelen [17,18]. In the first step the oxidation proceeds using lattice oxygen of the V-oxide which then needs to be replaced in a second step, the reoxidation process. Despite the application of numerous experimental techniques, on an atomic scale the picture of the catalytic surface processes is still rather incomplete. Theoretical studies, UHV-type investigations and the introduction of single crystalline model systems such as VO_x/α-TiO_2(1 1 0) aimed at bridging this gap [12–14,16,19].

Here we follow a different approach by studying the behavior of submonolayer VO_x layers on a metallic support during reaction conditions, instead of on an oxidic support. The concept of studying oxides on a metallic support instead of a conventional catalyst, where metals are supported by an oxidic support, has been termed inverse catalyst approach. This concept has been applied to prepare and characterize the interfacial metal/metal oxide sites, which supposedly play the essential role for the catalytic activity [20–24]. Moreover, the inverse catalyst concept has been applied as a preparation method for generating catalysts with promising properties.

Industrially, the partial oxidation of methanol to formaldehyde is catalyzed by oxide supported vanadium and/or molybdenum oxide catalysts in the so-called "formox" process [6,7]. In this study we investigate the redistribution dynamics of submonolayer vanadium oxide films on Rh(1 1 1) during the partial oxidation of methanol, covering a pressure range from UHV up to the 10^{-2} mbar range. Also with our model catalyst formaldehyde is the main reaction product for temperatures above 770 K in the 10^{-4} mbar range. Even though metal supported vanadium oxide films have no practical application, they represent an instructive model system to investigate reaction induced redistribution dynamics due to the higher VO_x mobility on metal surfaces compared to oxide surfaces. The results obtained may furthermore be relevant for understanding a group of phenomena summarized under strong metal support interactions (SMSI) [25,26]. Essentially, SMSI describes a wetting of metal particles by the oxidic support under reaction conditions.

With photoemission electron microscopy (PEEM), a newly developed near ambient pressure low-energy electron microscope (NAP-LEEM [27]) and its conventional variant (LEEM) we have been able to follow the reaction dynamics from UHV up to the 10^{-2} mbar range, thus bridging a large part of the pressure gap in catalysis. It turned out that the dynamics of the system are determined by large gradients in the oxygen coverage on the metallic and the oxide covered parts of the surface. These gradients give rise to a redistribution dynamics of VO_x on the substrate that varies strongly with the pressure from nearly static conditions to turbulent behavior. The strong dependence of the redistribution dynamics on the total pressure highlights the importance of in situ and operando studies in heterogeneous catalysis.

2. Materials and methods

2.1. Sample preparation

The Rh(1 1 1) single crystal (MaTeck GmbH), used as substrate for VO_x catalysts, was cleaned by repeated cycles of Ar^+ ion sputtering (20 min, 1 keV, 2–4 μA) and oxidation (20 min, $1 \cdot 10^{-6}$ mbar

O_2, 970 K), followed by a final flash annealing step (1300 K). The absence of impurities after cleaning was ensured by Auger electron spectroscopy (AES) in the PEEM experiments. A characteristic (2 × 2) LEED pattern after exposure to O_2 in the 10^{-8} mbar range was used as an indication of a clean surface during the LEEM experiments. A scanning Auger electron microscopy analysis of the VO_x/Rh(1 1 1) sample used for the NAP-LEEM experiments, performed after the sample has been transferred through air in a separate UHV chamber, yielded no contaminations except a small trace of carbon.

In the PEEM and LEEM experiments, ultrathin films of vanadium oxide are prepared by "reactive evaporation" [28]. V is evaporated from a high purity V rod (Goodfellow) in $2 \cdot 10^{-7}$ mbar O_2 by means of electron beam bombardment. During deposition the Rh (1 1 1) substrate was held at 670 K. After deposition, the temperature and oxygen pressure were maintained for further ten minutes, before the sample was cooled down in oxygen. In the NAP-LEEM experiments, V was deposited in vacuum at room temperature. The NAP-LEEM experiments were therefore started with a metallic V film. Preceding PEEM experiments conducted in the 10^{-4} mbar range with a Rh(1 1 1) surface covered with a submonolayer amount of metallic V and a surface covered with VO_x films deposited by reactive evaporation (same amount of V) verified that no differences with respect to pattern formation are found.

A V deposition rate calibration was achieved by a LEED. Submonolayer films (θ_V < 0.6–0.7 MLE) of VO_x exhibit a ($\sqrt{7} \times \sqrt{7}$)R1 9.1° LEED pattern. This pattern vanishes after a V coverage of 0.6 – 0.7 MLE is deposited, as has been determined with STM [28]. In NAP-LEEM, the same V evaporator as in the LEEM and PEEM experiments was used; the deposition rate was extrapolated, taking into account the different distance between evaporator and sample surface.

2.2. PEEM experiments

The UHV system is equipped with a four-grid low-energy electron diffraction (LEED) optics, an Auger electron spectrometer (AES), a differentially pumped mass spectrometer (QMS), and a PEEM. In PEEM, the sample is illuminated with photons emitted from a deuterium discharge lamp (Heraeus D 200 F). This lamp has a broad spectral distribution around a photon energy of 6 eV. The ejected photoelectrons are accelerated and projected onto an image intensifier unit [29]. Primarily, PEEM images the local work function. Areas of low work function appear as bright areas in PEEM, whereas areas of high work function appear as dark area. The Rh(1 1 1) single crystal was attached to a sample holder by two Ta wires, spot welded to the sides of the crystal. Heating up to 1030 K was achieved by passing current through these wires. Temperature measurement was conducted with a K-type thermocouple spot welded to the backside of the crystal.

Reaction rates were measured with a differentially pumped QMS. The QMS was separated from the main chamber by a nozzle with 6 mm diameter opening. In this way it was ensured, that all molecules have hit the sample surface prior to detection. Gases were introduced via a dedicated gas inlet system, equipped with feedback-controlled mass flow regulators, ensuring a constant gas phase composition over several hours. The total pressure was measured with an ionization manometer; different ionization cross sections of the gases were not taken into account (uncorrected pressure).

The freshly prepared VO_x catalysts were exposed to CH_3OH and O_2 gas mixtures with partial pressure ratios ranging from 3:1 (reducing) to 1:3 (oxidizing). Then the samples were heated from 300 K to 1030 K with 0.5 K/s. Afterwards the sample was cooled down with 0.5 K/s in a continuous gas flow to room temperature. For the reaction rate measurements, freshly prepared VO_x catalysts

were heated with 0.5 K/s from 300 K to 1030 K in front of the QMS nozzle.

2.3. LEEM experiments

For conventional LEEM experiments a SPELEEM (Elmitec), equipped with a LaB$_6$ cathode as electron source, was operated at 15 kV acceleration voltage. Before being backscattered at the sample surface, electrons are decelerated to low kinetic energies (0 – 200 eV). Inelastically scattered electrons are filtered out, and the reflected beam is projected onto a microchannel plate for image intensification. LEEM images are recorded by a CCD camera. Depending on the lens settings, either real space images can be obtained at various magnifications, or low-energy electron diffraction (LEED) can be performed.

Due to the strong interaction of the low-energy electrons with the sample, the information depth of LEEM is only a few atomic layers [30,31]. In the mirror electron microscopy mode (MEM), the information depth is even lower, since the probing electron beam is reflected in front of the surface. Real space imaging is possible with about 10 nm lateral resolution and mesoscopic fields of view of up to 100 μm can be reached. In μLEED mode, the illuminating electron beam can be restricted by apertures to probe sample regions of 0.25, 1, and 5 μm in diameter, allowing a local structural characterization of the surface.

While cleaning of the substrate was performed in a separate preparation section of the same UHV system, VO$_x$ film growth was conducted in situ in the analysis chamber. For comparability, oxygen and methanol were dosed with the same gas inlet system as used in the PEEM experiments described above.

2.4. NAP-LEEM experiments

A detailed description of the used NAP-LEEM can be found in reference [27]. In NAP-LEEM, a small capillary in the optical path of the microscope separates the reaction cell from the other parts of the microscope. Differential pumping ensures that UHV conditions are maintained in the imaging part of the microscope, while the pressure in the reaction cell is as high as 0.1 mbar.

In the NAP-LEEM experiments, sample cleaning and V film deposition were performed in a separate preparation chamber. Afterwards the sample was transferred in vacuo into the reaction cell of the microscope. Gases were dosed through the same gas inlet system as used in the PEEM and LEEM instruments. The total pressure of the reaction gas mixture was measured with a Pirani gauge (Leybold TM 210 S) in the gas inlet system. The pressure inside the reaction cell was calculated from a calibration measurement performed with a home-built Pirani-type gauge mounted on a sample holder and placed in the measurement position within the reaction cell. In addition, the partial pressures of the reactants were followed with a QMS located in the first differential pumping stage of the microscope.

The sample was heated by a boron nitride (BN) heater, on which the Rh(1 1 1) crystal was mechanically pressed by a titanium cap. Ti was used as cap material to avoid contamination of the sample at high oxygen partial pressure and temperature. The temperature was measured with a C-type thermocouple attached to the backside of the BN heater.

In order to observe pattern formation, the V/Rh(1 1 1) sample was kept at room temperature until a continuous flow of reactants, resulting in a gas phase composition of 0.01 mbar CH$_3$OH and 0.01 mbar O$_2$, was established. Afterwards the sample was heated up slowly within about 30 min from room temperature to 670 K and held at this temperature for further observations. After completion of the experiment, the sample was cooled down to room temperature in a continuous gas flow, and transferred through

air in a separate UHV system for an AES analysis. The scanning Auger electron spectroscopy measurement showed no indications for contamination except small amounts of carbon.

2.5. Density functional theory calculations

Structures were optimized using the generalized gradient approximation to exchange and correlation effects after Perdew, Burke, and Ernzerhof (PBE) [32]. Projector augmented wave pseudopotentials as implemented in the Vienna ab initio simulation package (VASP) were used together with a kinetic energy cutoff of 600 eV to describe the electron-ion interaction [33,34]. Rh and V pseudopotentials included the semi-core p states, resulting in 15 and 11 valence electrons, respectively. Slab models to describe VO$_x$ clusters and films deposited on the Rh(1 1 1) surface used four atomic metal layers, the lowest one being fixed in bulk positions, and a vacuum distance of ca. 10.5 Å. Monkhorst-Pack [35] k meshes centered at the Γ point were used. A (7 × 7) mesh was applied to the (2 × 2) cell of Rh(1 1 1). The SCF break criterion was 10^{-6} eV and atomic positions were optimized by virtue of a maximum force criterion of 0.02 eV/Å, which is equivalent to ca. 3.8×10^{-4} Hartree/Bohr. The Gaussian smearing method and a sigma of 0.1 eV was used. Total energies were obtained as single points using the so-called tetrahedron method with Blöchl corrections [36]. Dispersion-type corrections were obtained using the Grimme D2 method employing the global scaling of 0.75 optimized for the PBE functional and default C$_6$ and R$_0$ parameters for V, O, and Rh (see Table 1) [37,38].

The phase diagram for various adsorption systems is constructed using statistical thermodynamics [39]. In short, the change in surface free energy was calculated according to

$$\Delta\gamma = \frac{1}{A}(\Delta G - n\Delta\mu_V - m\Delta\mu_O)$$

with

$$\Delta G = G[V_nO_m \cdot Rh(111)] - nG[V] + \frac{m}{2}G[O_2] - G[Rh(111)]$$

where A is the surface area of the unit cell and $\Delta\mu_V$ and $\Delta\mu_O$ represent the change in chemical potential of vanadium and oxygen, respectively. The references for $G[V]$ and $G[O_2]$ are bulk vanadium and an isolated oxygen molecule, respectively. Vibrational contributions to free energies were obtained by diagonalizing a partial, mass-weighted matrix of second derivatives with respect to the three Cartesian degrees of freedom of each atom. This partial Hessian was obtained via finite differences of (analytic) Hellmann-Feynman forces (gradients) displacing V and O atoms by ±0.015 Å [40,41]. Entropic contributions in bulk vanadium and the Rh(1 1 1) surface were neglected (i.e., total DFT energies were used).

3. Results and discussion

In the sub-monolayer range, vanadium oxide on Rh(1 1 1) forms a number of well-ordered two-dimensional phases, which have been thoroughly characterized [22,28,42,43]. As illustrated by Fig. 1a, these structures can be built up as a 2D-network in which VO$_n$ polyhedra (n = 3–6) as structural units are connected by sharing oxygen corner atoms [44]. As long as the V coverage remains below $\theta_V \approx 0.6–0.7$ MLE, the network does not exceed one monolayer height (MLE $\hat{=}$ monolayer equivalent; 1 MLE contains the same number of V atoms as the topmost Rh(1 1 1) layer).

Ordered V-oxide overlayers are prepared on Rh(1 1 1) by reactive deposition of varying amounts of V ($0.1 \leq \theta_V < 0.6$ MLE) in $2 \cdot 10^{-7}$ mbar O$_2$, thus the experiments are performed with sub-monolayer VO$_x$ coverages. Upon heating the VO$_x$ covered surface in a methanol and O$_2$ atmosphere, the initially homogeneous state

Table 1
C_6 (J nm^6/mol) and R_0 (Å) parameters employed within the Grimme D2 dispersion-correction.

Atom	C_6	R_0
Rh	24.670	1.639
V	10.800	1.562
O	0.700	1.342

of the surface (homogeneous on the length scale of the PEEM instrument, which has a resolution of about 1 μm) is lifted and a phase separation into VO$_x$-rich and VO$_x$-depleted areas takes place, associated with an activation of the catalyst [45]. In the 10^{-7} mbar range, starting from 970 K for a gas phase composition of 3 × 10^{-7} - mbar methanol and 1 × 10^{-7} mbar oxygen and 1020 K for 1 × 10^{-7} - mbar methanol and 3 × 10^{-7} mbar oxygen, the phase separation leads to static, several 100 μm wide regions of vanadium oxide covered area, which are separated by a sharp interface from the surrounding Rh(1 1 1) surface. A variation of the gas phase composition shifts the onset temperature of pattern formation to higher values for more oxidizing conditions. But different from the experiments conducted at higher total pressure, no marked difference in pattern formation is found. In the 10^{-4} mbar range macroscopic stripes evolve, which then transform at 970 K into circular VO$_x$ islands (please refer to SI2 and 3). The term macroscopic refers here and in the following to pattern length scales of tens to several hundreds of μm, as imaged with our PEEM instrument (500–1100 μm field of view). This process results in a partial dewetting of the VO$_x$ film, which is schematically depicted in Fig. 1b. With increasing pressure, the length scale of the island pattern gets smaller (please refer to SI1). During the whole redistribution process the VO$_x$ structures remain two-dimensional.

In preceding studies, it has been shown that the VO$_x$ islands exhibit two remarkable properties [45–47]: (i) under reaction conditions, nearby VO$_x$ islands approach each other and coalesce. Turning off the supply of one reactant instantly freezes any movement of the oxide islands. (ii) The VO$_x$ islands exhibit a substructure, appearing as a bright core and a dark outer ring in PEEM. PEEM and LEEM images showing this substructure of VO$_x$ islands in the 10^{-4} mbar range are displayed in Fig. 2. The substructure develops if the island size exceeds a critical radius, which depends on the reaction conditions. A higher amount of methanol in the gas phase favors the development of a reduced core in the center of the VO$_x$ islands. As was shown with micro-X-ray photoelectron spectroscopy (μXPS) in a preceding study, the bright island cores in the PEEM image contain vanadium in a more reduced state, i.e.

with V^{3+} species dominating. In the surrounding outer dark ring V^{4+} is prevalent [45]. It has to be noted, that the oxidation states here are only formal oxidation states deduced from comparison with core level shifts of thick VO$_x$ films.

For comparison annealing experiments with pure oxygen and pure methanol have been conducted. If a freshly prepared VO$_x$/Rh(1 1 1) catalyst is exposed to pure oxygen in the 10^{-4} mbar range, macroscopic VO$_x$ islands form, but no movement of these islands towards each other, as occurring during methanol oxidation, is observed. If instead a fresh VO$_x$/Rh(1 1 1) catalyst is heated to 1030 K in pure methanol, no pattern formation can be observed in PEEM. Without the stabilizing presence of oxygen, however, the diffusion of V into the subsurface region of the Rh(1 1 1) crystal occurs, as indicated by a loss in the V AES signal. Furthermore the reduction of VO$_x$ shows up in PEEM by a strong brightness increase due to the loss of oxygen and the resulting work function decrease.

3.1. Catalytic activity

The total oxidation of methanol yields the reaction products CO$_2$ and H$_2$O according to

$$CH_3OH + {}^3/_2 O_2 \rightarrow CO_2 + 2 H_2O \tag{R1}$$

Formaldehyde, CH$_2$O, is generated in the partial oxidation of CH$_3$OH:

$$CH_3OH + \tfrac{1}{2} O_2 \rightarrow CH_2O + H_2O \tag{R2}$$

In addition, CO is found as shown in the rate measurements in Fig. 3, produced either by CH$_3$OH decomposition or by incomplete oxidation of CH$_3$OH according to

$$CH_3OH + O_2 \rightarrow CO + 2 H_2O \tag{R3}$$

As indicated in the scheme of Fig. 1b, the total oxidation proceeds mainly on the bare metal surface, whereas CH$_2$O production is restricted to VO$_x$-covered regions. Considerable amounts of CO are formed on both, on the Rh(1 1 1) surface and on the VO$_x$ covered Rh(1 1 1). The different catalytic activity is reflected in the reaction rates measured on an unpromoted Rh(1 1 1) surface and on a Rh(1 1 1) surface covered with 0.2 MLE VO$_x$ under reducing (1 × 10^{-4} mbar oxygen and 3 × 10^{-4} mbar methanol) and oxidizing (1 × 10^{-4} mbar oxygen and 1 × 10^{-4} mbar methanol) reaction conditions. The data in Fig. 3 show that the onset of pattern formation indicated by arrows in the diagrams is connected with a sharp increase in the reaction rates, which is particularly pronounced in
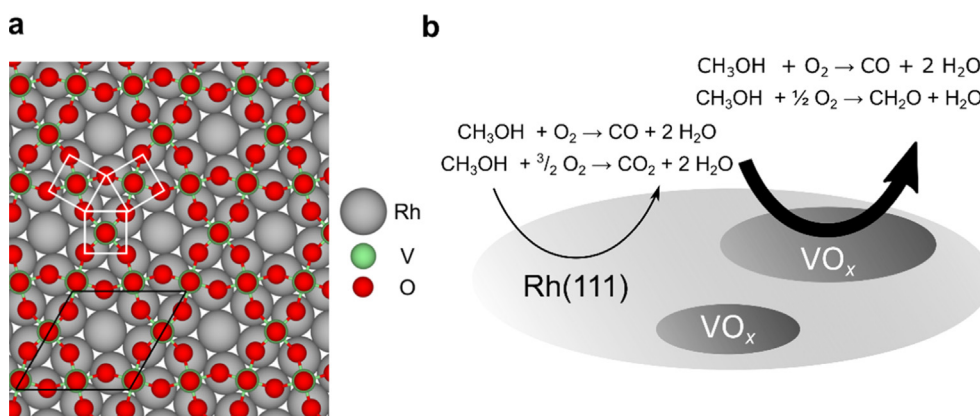
Fig. 1. a) Structure model for the ($\sqrt{7} \times \sqrt{7}$)R19.1° vanadium oxide phase on Rh(1 1 1) with a VO$_3$ composition and θ_V = 0.43 MLE [28]. The unit cell is indicated in the model as well as a VO$_5$ pyramid as the structural unit. b) Sketch of catalytic vanadium oxide "microreactors" on a Rh(1 1 1) surface during catalytic methanol oxidation, as observed in the 10^{-4} mbar range. The main catalytic reactions on Rh and vanadium oxide are indicated.
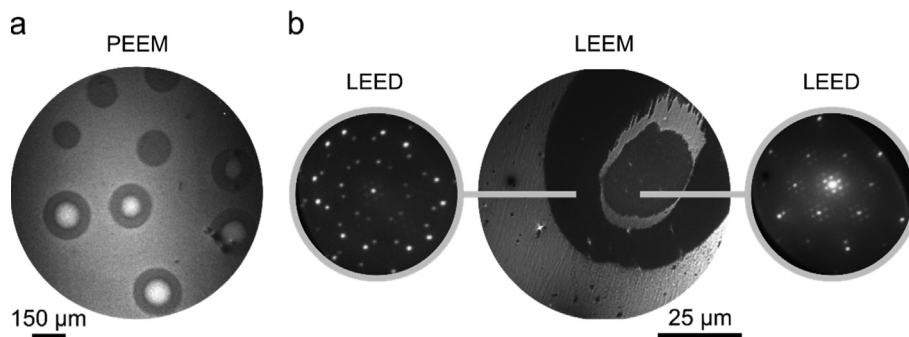
Fig. 2. Substructure of circular VO$_x$ islands under reaction conditions, as demonstrated by PEEM and LEEM images. a) PEEM image recorded at 1030 K in an atmosphere of $3 \cdot 10^{-4}$ mbar CH$_3$OH and $1 \cdot 10^{-4}$ mbar O$_2$. b) LEEM image recorded at 2 eV and corresponding LEED patterns acquired at 50 (left) and 65 eV (right) in $1 \cdot 10^{-4}$ mbar CH$_3$OH and $1 \cdot 10^{-4}$ mbar O$_2$ at 1030 K.
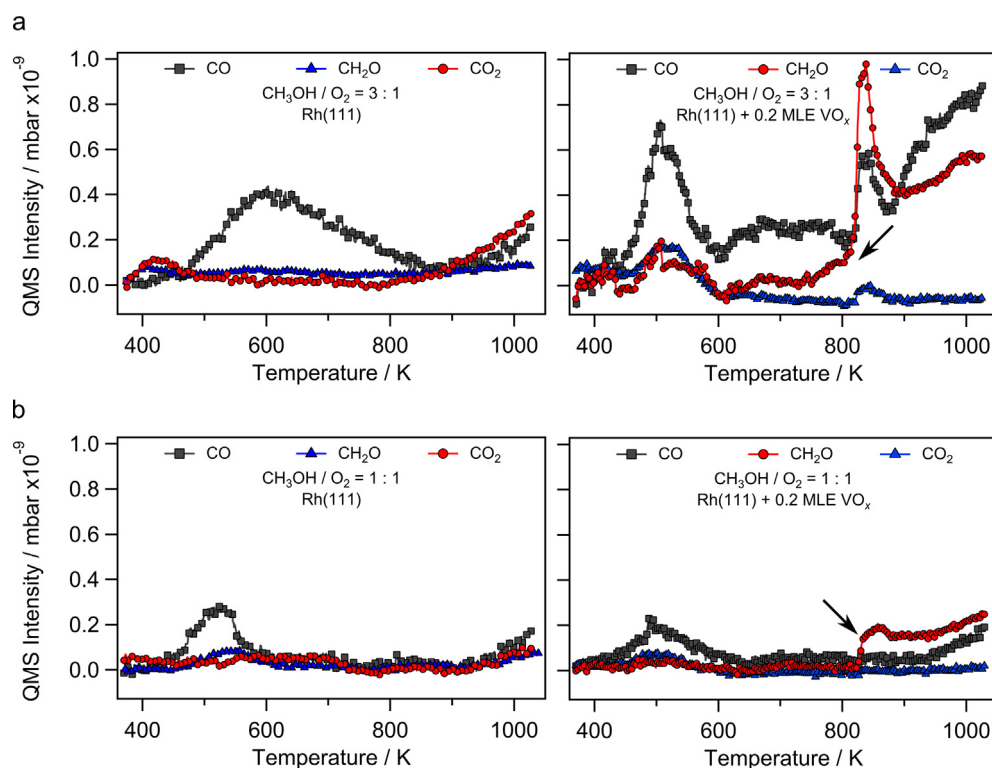
Fig. 3. Reaction rates measured on an unpromoted Rh(1 1 1) surface (left) and on a Rh(1 1 1) surface covered with 0.2 MLE VO$_x$ (right). Shown are the heating (VO$_x$/Rh(1 1 1)) and cooling (Rh(1 1 1)) branches of temperature programmed reaction experiments (0.5 K/s) with freshly prepared catalysts. a) CO (mass 28), formaldehyde (mass 30) and CO$_2$ (mass 44) partial pressures measured in an atmosphere of 1×10^{-4} mbar oxygen and 3×10^{-4} mbar methanol. b) Partial pressures of the reaction products measured in 1×10^{-4} mbar oxygen and 1×10^{-4} mbar methanol. The black arrows indicate the onset temperature of pattern formation in PEEM. For the calculation of the partial pressures from the QMS measured ion currents, the ionization probability and the fragmentation patterns of the individual molecules have been taken into account.

formaldehyde production. On the unpromoted Rh(1 1 1) surface the formaldehyde production rate is not zero but the rate is considerably smaller than on the surface partially covered with VO$_x$. One notes that under reducing conditions the catalytic activity on Rh (1 1 1)/VO$_x$ and the jump at ≈ 820 K are considerably higher than under oxidizing conditions. Also only under reducing conditions we observe a substructure of a reduced core region in the center of the VO$_x$ islands for T < 1000 K (s. Fig. 2a). The development of the reduced core can accordingly be associated with a state of high catalytic activity. Under oxidizing reaction conditions, a reduced core can also be obtained but only after heating beyond 1000 K and only for large islands (please refer to SI2).

Besides the gas phase composition, the catalytic activity depends also on the vanadium oxide coverage. For coverages up to roughly 0.5 MLE the formaldehyde production rate increases with increasing amount of V-oxide, and the onset temperature of formaldehyde production shifts to lower temperature by roughly 20 K. The completion of the first VO$_x$ surface layer drastically reduces the formaldehyde production rate. At the same time, no redistribution dynamics are seen in PEEM for closed VO$_x$ films or multilayers.

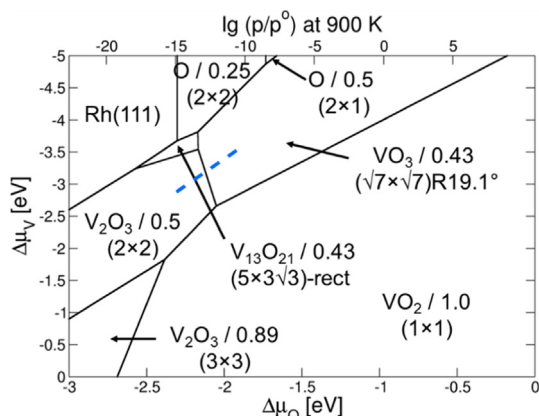### 3.2. Reaction dynamics at 10^{-4} mbar

The development of a substructure consisting of a reduced core and an outer, oxidized ring in the vanadium oxide islands is a consequence of how the oxygen is supplied to the VO$_x$ islands. The oxygen sticking coefficient is low on the V-oxide islands but high on the metallic Rh(1 1 1) surface ($s(O_2) \approx 0.2$ at 300 K) [48,49]. Consequently, oxygen is mainly supplied by dissociative adsorp-
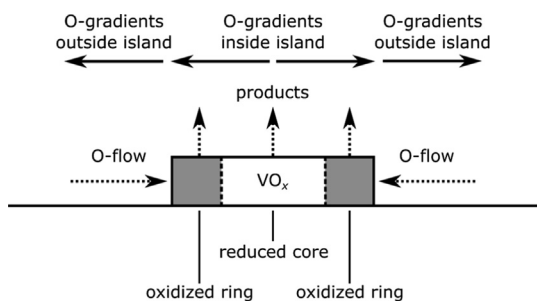
Fig. 4. Schematic drawing explaining the existence of oxygen gradients inside and around VO_x islands supported on Rh(1 1 1) during catalytic methanol oxidation. For details please refer to the text.

tion of O_2 on the surrounding metallic Rh(1 1 1) surface, from where O_{ad} is diffusively transported to the VO_x islands. Since the main catalytic activity, CH_2O production, takes place inside the VO_x islands, these VO_x islands can be considered as catalytic "microreactors". As depicted in Fig. 4, they act as sinks for diffusing oxygen, thus causing a gradient in the chemical potential of oxygen around each VO_x island. Furthermore, also inside the islands a gradient in the chemical potential will develop, because oxygen is supplied only from the island boundary, from where it has to diffuse inside, while being continuously consumed by the oxidation reaction. The chemical potential of oxygen and thus the thermodynamic conditions for the stability of different VO_x phases will therefore change continuously as one moves from the boundary of a VO_x island towards the core.

With DFT, the phase diagram of the 2D-phases of VO_x on Rh (1 1 1) has been calculated for T = 900 K. The result is shown in Fig. 5. The stable phase we obtain after preparation of a V-oxide submonolayer is the $(\sqrt{7} \times \sqrt{7})$R19.1° structure (henceforth simply denoted as "$\sqrt{7}$"), in which V is in a formal oxidation state between +4 and +5 [28,43]. The $(\sqrt{13} \times \sqrt{13})$R13.8° has been observed and discussed by Kresse and Netzer et al. to be energetically degenerate [28]. In our work only the $\sqrt{7}$ was observed and therefore, the $(\sqrt{13} \times \sqrt{13})$R13.8° was not included in the calculation of the phase diagram. With μLEED the $\sqrt{7}$ has also been identified as the structure of the outer ring of a VO_x island, as shown in Fig. 2b. Vanadium there is in a highly oxidized state, in agreement with the results of a previous μXPS study [45]. According to the phase diagram one should expect for the reduced phase

in the island center either a (2×2) or a $(5 \times 3\sqrt{3})$-rect structure. Experimentally, with μLEED, we could identify a $(\sqrt{3} \times \sqrt{3})$-Moiré pattern for the reduced core, as indicated in Fig. 2b. This structure has, to our best knowledge, not been described before and therefore no structural models exist.

The coexistence of different VO_x phases in the interior of a VO_x island leads, in connection with the oxygen gradients generated by a catalytic reaction, to complex dynamics. This is demonstrated by the LEEM images in Fig. 6a (please refer to SI4 for a LEEM video of an oscillating island). Despite constant reaction conditions in the 10^{-4} mbar range, the VO_x island undergoes a periodic expansion and contraction with a period of approximately 30 s. The left frame shows the island with a dark core, separated by a bright band from
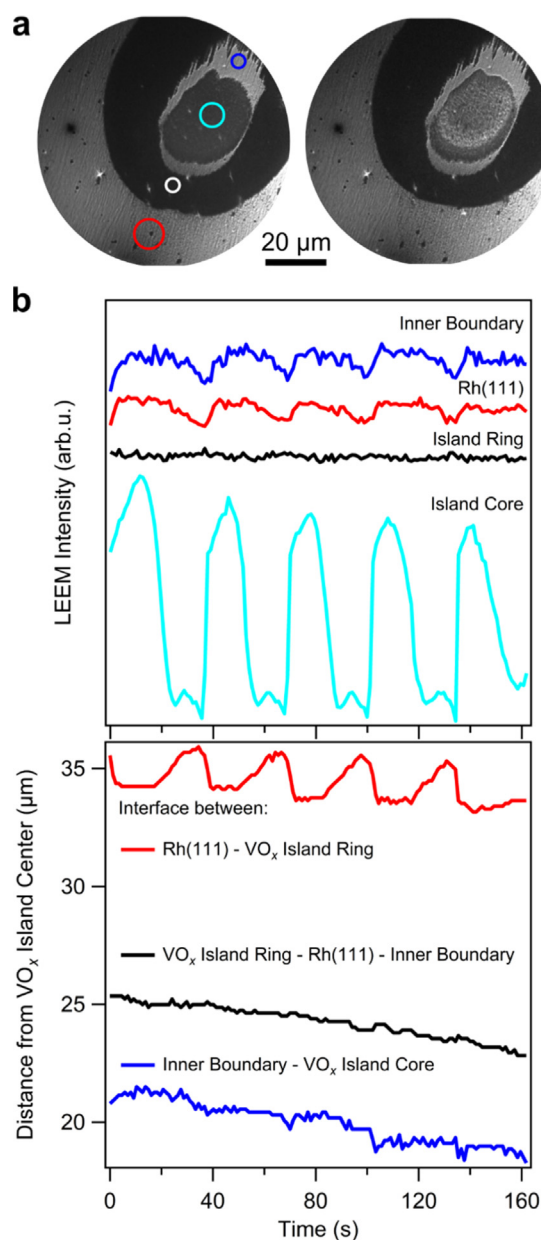
Fig. 6. Oscillation of VO_x islands during methanol oxidation in the 10^{-4} mbar range. a) LEEM images, showing a VO_x island with the core region in its oxidized (left) and its reduced (right) state. b) Local LEEM intensity (top) and the position of the different interfaces (bottom) are shown as a function of time. The areas over which the LEEM intensity is recorded are indicated by colored circles in the left LEEM image (a). The LEEM image is recorded at 2 eV in $1 \cdot 10^{-4}$ mbar CH_3OH and $1 \cdot 10^{-4}$ mbar O_2 at 1030 K.

Fig. 5. DFT phase diagram of 2D VO_x phases with a coverage of $\theta_V \leq 1$ MLE. The chemical potential of oxygen has been translated into a pressure scale based on tabulated data for 900 K. The V coverages in MLE as well as the surface structure are given with the composition of the corresponding oxide phase. The dashed blue line indicates a possible phase transition during the island oscillations described in the text.

the outer dark ring. The brightness variations and interface positions in the core region are displayed in Fig. 6b. When the outer ring starts to expand, shortly after reaching the maximum size with approximately 5%/1.5 μm increase in radius, the core region rapidly transforms from dark into bright via propagating fronts. These fronts nucleate in the interior of the core and propagate outwards. Simultaneously with the rising intensity of the core, the outer ring starts to contract. Shortly after the contraction stops, a second front transforms the bright core back into the original dark grey area. This second front nucleates at the rim of the inner core and propagates inwards from there again, resulting in a periodic behavior.

In such a "breathing cycle" the island changes its area by approximately 10% or 350 μm^2. The variations in the area are mainly caused by expansion/contraction of the outer ring, while the size of the core region and the bright band between core and outer ring is rather constant, as can be seen in the second graph of Fig. 6b. Because the transformations in the core region proceed via reaction fronts, we can associate the brightness changes of the core region with an oxidation and reduction process of the VO$_x$ phase.

Since small variations in the island size trigger transformations from the oxidized core to the reduced core and vice versa, the island size evidently varies around the critical radius for the formation of a reduced core. The existence of a critical radius for the oscillations is further evidenced by the fact, that the coalescence of the oscillating island with another island in the surrounding terminates the size oscillations. This is simply a consequence of the island radius being then much larger than the critical radius.

In the following, we assume that we move along the dashed blue line indicated in the phase diagram of Fig. 5 during the transformations of the core region. The formal oxidation state of the core accordingly changes between V^{5+}/V^{4+} of the $\sqrt{7}$ with VO$_3$ composition and V^{3+} of the (2 × 2) with V$_2$O$_3$ composition; both is in agreement with preceding μXPS results [45]. (A VO$_3$ composition is not in contradiction to the maximum oxidation state of +5 for V, since the basal O atoms in the two-dimensional vanadium oxide layer are shared with the Rh(1 1 1) substrate.)

Here, we tentatively sketch a mechanism for an oscillatory cycle of a VO$_x$ island:

We start with the VO$_x$ island at maximum size and with the core still being in the oxidized state. Due to the long distance that diffusing oxygen atoms have to cover before reaching the core, the core region is no longer supplied with sufficient oxygen to maintain a V^{4+} state. A partial net reduction of the core region will therefore set in. Since the surface density of V atoms in the reduced state is about 15% larger than in the oxidized state, extra V atoms are needed, which are taken from the outer ring. Consequently, the VO$_x$ island shrinks. (ii) With the shorter diffusion length for oxygen atoms, the oxygen coverage in the core region will rise, thus finally triggering the transformation to the oxidized state. Due to the lower density of V atoms in the oxidized state, V atoms are expelled from the core region. V is transported from the core to the outer ring, which grows, thus completing an oscillatory cycle. The transport of V inside the VO$_x$ islands may occur via mobile V-oxo complexes or via diffusion of the naked metal ion.

For explaining pattern formation diffusion is essential; the diffusion length of the rate-limiting species should be compatible with the experimentally observed length scales [50,51]. In particular, in island coalescence the distance of ≈ 100 μm at which two islands start to interact should be determined by a fast diffusing species. Hydrogen is known to diffuse rapidly on a Rh(1 1 1) surface, but due to the very short residence time of atomic hydrogen at 800–1000 K, a diffusion length of less than 1 μm results. This value is obtained from the diffusion parameters for H/Rh(1 1 1) with $D_0 = 1 \times 10^{-3}$ cm^{2}s^{-1} and $E_a = 18.0$ kJmol^{-1}, using the adsorption energy of 71 kJmol^{-1} of adsorbed hydrogen for estimating the surface residence time of atomic hydrogen on Rh(1 1 1) [52,53]. From STM data of O/Pt(1 1 1) and from a DFT study of O/Rh (1 1 1) one obtains for oxygen diffusion on Rh(1 1 1), putting in a surface residence time of adsorbed oxygen of 0.1 s at 1000 K, a diffusion length in the range of 10–20 μm [53–55]. This is just in the range of 10–100 μm where two neighboring VO$_x$ islands start to interact, and this is also the range over which gradients in the oxygen coverage on the Rh(1 1 1) area, surrounding the VO$_x$ islands, extend under reaction conditions [45].

On the free Rh(1 1 1) surface mass transport of V occurs via small, mobile V$_n$O$_m$ clusters; V$_6$O$_{12}$ clusters on Rh(1 1 1) have been identified in STM and their diffusivity is well compatible with the experimentally observed evaporation rate of macroscopic VO$_x$ islands under reaction conditions [42]. For diffusion inside the VO$_x$ islands no experimental data exist but the existence of a reduced core, and of large differences in the oxygen concentration within an island suggests, that oxygen diffusion should play a major role. This conclusion also agrees with the general picture of VO$_x$ islands acting as catalytic microreactors, i.e. as a sink for oxygen supplied diffusively from the bare Rh(1 1 1) surface surrounding the islands. The size oscillations of VO$_x$ islands shown in Fig. 6 clearly demonstrate, that a mass transport of V atoms inside the VO$_x$ islands has to be involved too. Such a mass transport of V also follows as a consequence of the Onsager relations, which require that a gradient in the chemical potential of oxygen has to be connected with a corresponding gradient in the chemical potential of vanadium [50,51]. In addition to surface diffusion of vanadium, one should also take into account the possibility of a reversible segregation of V into subsurface sites of the Rh(1 1 1) crystal [43,56]. This possibility appears rather unlikely since even small amounts of oxygen are known to stabilize vanadium oxide on the Rh(1 1 1) surface up to temperatures around 1000 K. The μXPS measurements previously reported [45] indicate a considerable amount of oxygen in the outer oxidized ring of a macroscopic VO$_x$ island, as well as in the reduced core. Under similar conditions, however, vanadium diffuses into subsurface layers during catalytic methanol oxidation on VO$_x$/Rh(1 1 0) [57,58].

The mechanism sketched above should be considered as tentative, because not all of the phases in the island core and in the region between core and outer ring have been identified. Quite generally in experiments at high temperature, here between 800 and 1000 K, and under reaction conditions, thermally and reaction-induced disorder render an identification of the different phases by μLEED difficult. Also the different diffusion kinetics of oxygen and V species might contribute to the instability of the islands.

3.3. Reaction dynamics at 10^{-2} mbar

Using the newly developed NAP-LEEM, the pressure is raised to 10^{-2} mbar. The dynamics of the reaction again change drastically (please refer to SI 4 for a NAP-LEEM video of the reaction dynamics). After preparation of a homogeneous V film with $\theta_V = 0.2$ MLE at 300 K, the sample was heated up to 670 K within 30 min in an atmosphere of methanol and oxygen with a 1:1 ratio of the reactants and a total pressure of 2×10^{-2} mbar. The sequence of NAP-LEEM images in Fig. 7a illustrates the development of the VO$_x$ submonolayer film under NAP conditions during heating up the sample. Initially, circular oxide islands form, consisting of an outer ring and an inner core, similar to the experiments conducted in the 10^{-4} mbar range. At elevated temperature, at about 650 K, we observe that first the outer ring of the VO$_x$ islands disintegrates, while the core region remains intact. The outer ring expands, followed by the nucleation of bright areas first at the inner boundary to the core region, and a few seconds later at the outer boundary.
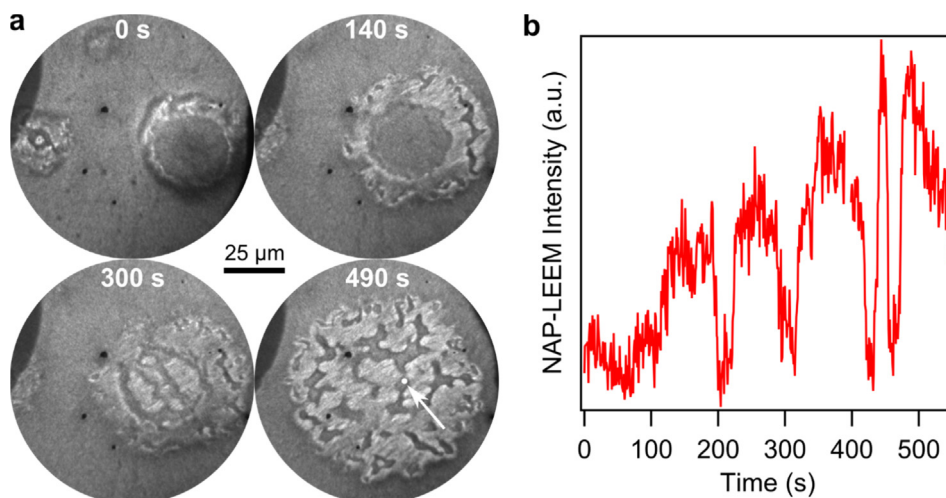
Fig. 7. NAP-LEEM images showing VO$_x$ islands during the transition from a core-ring structure to turbulent dynamics. a) Series of NAP-LEEM images acquired at 3.1 eV between 650 and 670 K with a field of view of 100 μm. The gas phase consists of 1 · 10^{-2} mbar O$_2$ and 1 · 10^{-2} mbar CH$_3$OH. In the images the time elapsed since the beginning of the island disintegration is indicated. b) Local NAP-LEEM intensity as a function of time recorded in the circular white area of 3 μm diameter, indicated by a white arrow in the last NAP-LEEM image of (a).

As the outer ring disintegrates, dark channel-like islands develop that start to meander on the surface. In the second stage, at even higher temperature of about 670 K, these dark islands also develop in the core region. The dark islands possess long extensions which often break and become reconnected to other dark islands. As illustrated by the time series of the local LEEM intensity in Fig. 7b, a rather violent turbulent dynamics evolves. From the behavior upon variation of the methanol partial pressure, it is evident that the bright phase in the LEEM images represents the oxidized state of the surface and the dark phase the reduced state.

In our experiments, a stable stationary distribution of the different vanadium oxide phases cannot be maintained in the 10^{-2} mbar range, and a turbulent VO$_x$ redistribution is observed instead. Several factors change when we increase the pressure from 4 × 10^{-4} to 0.02 mbar. Due to the higher gas pressure, the reaction can no longer be considered as strictly isothermal. For example, the threshold in pressure at which the reaction heat in catalytic CO oxidation on Pt single crystal surfaces is no longer negligible and causes a temperature rise lies in the 10^{-3} to 10^{-2} mbar range [59,60]. Temperature gradients might therefore evolve. Another factor contributing to the instability might be that higher pressures enhance the oxygen gradients between the V-oxide islands and the surrounding metallic phase.

3.4. Relation to real catalysis

When one compares the behavior of planar 2D-model systems with real catalysts, a seemingly obvious difference one considers usually is the three-dimensional nature of the real catalyst vs. the reduced dimensionality of the two-dimensional model catalyst. In the present case, however, this is not true since, according to the literature, VO$_x$ in its most active form is present as isolated V$_x$O$_y$-clusters or a monomolecular 2D-film. The metallic support vs. oxidic support will of course lead to much more pronounced differences in the oxygen gradients around the VO$_x$ islands on a metallic support due to fast oxygen adsorption kinetics on the metallic phase. However, due to the heterogeneity of the surface, gradients in the oxygen coverage should also develop on an oxidic support. One should therefore expect to see some similarities in the dynamic behavior of VO$_x$ on both types of supports.

For example, the sintering of VO$_x$ observed on real catalysts [61,62] might have a similar mechanistic origin as the island coa-

lescence we observe on Rh(1 1 1)/VO$_x$. A decrease of catalytic activity upon prolonged exposure to reaction conditions can often be explained by the sintering of submonolayer VO$_x$ clusters on oxidic supports during operation. Consequently, understanding the redistribution dynamics of VO$_x$ is of crucial importance. Recently, the redox dynamics of TiO$_2$ supported vanadium oxide catalysts were studied on the atomic scale using transmission electron microscopy [63]. A reversible order-disorder transition was observed in oxidation/reduction cycles of 0.5 and 2 monolayer thick VO$_x$ films, accompanied by a change in the V oxidation state and a considerably higher V mobility under reducing conditions. Our results are consistent with the reported reaction dynamics on oxidic surfaces. The turbulent behavior of VO$_x$ islands we already observe at 10^{-2} -mbar should even be much more pronounced at atmospheric pressure.

Furthermore vanadium is known to easily change its oxidation state between 5+ and 3+ during catalytic reactions. This is particularly true for ultrathin films of submonolayer coverage up to several layers deposited on both, metallic and oxidic supports [43,62,64]. In multilayer VO$_x$ films, often only the outermost VO$_x$ layer is fully oxidized, resulting in the simultaneous presence of V^{5+} species and V in a less oxidized state. A similar situation is present in our experiments. However, the here studied VO$_x$ model catalysts are of submonolayer thickness and the different oxidation states of V are present as 2D phases.

4. Conclusion

With the successful operation of a NAP-LEEM, the dynamics of a supported VO$_x$ catalyst could be followed from UHV up to the 10^{-2} mbar range. While nearly static VO$_x$ islands develop at low pressure (10^{-7} to 10^{-6} mbar range), interesting dynamics evolve with increasing pressure, showing an oscillatory breathing mode in the 10^{-4} mbar range until turbulent dynamics are obtained in the 10^{-2} mbar range. Clearly, depending on the pressure range qualitatively different dynamics are observed. The state of the surface is different in each pressure range thus nicely illustrating the meaning of the term "pressure gap".

The mechanistic elements behind the dynamic processes can be formulated as follows: With oxygen being diffusively transported to the "catalytic microreactors", oxygen gradients arise around the VO$_x$ islands, as well as inside the VO$_x$ islands. These conclusions

are in agreement with earlier work [45–47]. The oxygen gradients inside the VO_x islands cause a phase separation into distinct phases. A critical island size exists for this separation, which depends on the reaction conditions. The dependence of the thermodynamic stability of different VO_x phases on the island size can cause kinetic instabilities as evidenced by the oscillatory breathing of islands at 10^{-4} mbar. This last example demonstrates that besides oxygen diffusion, we also encounter a transport of vanadium inside the VO_x islands.

It is well established that catalysts are modified by a catalytic reaction. The NAP-LEEM experiments here demonstrate, that the catalyst is part of a violent dynamics, which continuously redistributes the V-oxide on the support material. Since the reactivity of oxidic surfaces is typically determined by structural defects, turbulent dynamics creating a large amount of structural defects, may actually be beneficial for enhancing catalytic activity.

For designing metal/oxide catalysts, it is essential not just to understand the static properties of adsorption sites, but to take into account the dynamic properties that develop under reaction conditions as well. For the metal/oxide systems considered here, the dynamics are mainly determined by large oxygen gradients between the different components of the catalyst. As we have demonstrated these dynamics give rise to a number of new and unexpected phenomena.

Author contributions

The manuscript was written through contributions of all authors. All authors have given approval to the final version of the manuscript.

Declaration of Competing Interest

The authors declare that they have no known competing financial interests or personal relationships that could have appeared to influence the work reported in this paper.

Acknowledgment

Appendix A. Supplementary material

Supplementary data to this article can be found online at https://doi.org/10.1016/j.jcat.2020.03.016.

References

[1] M. Flytzani-Stephanopoulos, L.D. Schmidt, Morphology and etching processes on macroscopic metal catalysts, Prog. Surf. Sci. 9 (1979) 83–111.

[2] T.-C. Wei, J. Phillips, Thermal and catalytic etching, in: D.D. Eley, W.O. Haag, B. Gates (Eds.), Advances in Catalysis, Academic Press, New York, N.Y., 1996, pp. 359–421.

[3] F. Tao, S. Dag, L.-W. Wang, Z. Liu, D.R. Butcher, H. Bluhm, M. Salmeron, G.A. Somorjai, Break-up of stepped platinum catalyst surfaces by high CO coverage, Science 327 (2010) 850–853.

[4] G. Prieto, F. Schüth, Bridging the gap between insightful simplicity and successful complexity: from fundamental studies on model systems to technical catalysts, J. Catal. 328 (2015) 59–71.

[5] R. Schlögl, Heterogeneous catalysis, Angew. Chem. Int. Ed. 54 (2015) 3465–3520.

[6] P. Forzatti, E. Tronconi, A.S. Elmi, G. Busca, Methanol oxidation over vanadia-based catalysts, Appl. Catal., A 157 (1997) 387–408.

[7] G. Reuss, W. Disteldorf, A.O. Gamer, A. Hilt, Formaldehyde, in: Ullmann's Encyclopedia of Industrial Chemistry, Wiley-VCH Verlag GmbH & Co. KGaA, Weinheim, Germany, 2000, p. 377.

[8] G.C. Bond, S.F. Tahir, Vanadium oxide monolayer catalysts - preparation, characterization and catalytic activity, Appl. Catal. 71 (1991) 1–31.

[9] K. Chen, A.T. Bell, E. Iglesia, The relationship between the electronic and redox properties of dispersed metal oxides and their turnover rates in oxidative dehydrogenation reactions, J. Catal. 209 (2002) 35–42.

[10] I.E. Wachs, Y. Chen, J.-M. Jehng, L.E. Briand, T. Tanaka, Molecular structure and reactivity of the group V metal oxides, Catal. Today 78 (2003) 13–24.

[11] N. Magg, Vibrational spectra of alumina- and silica-supported vanadia revisited: an experimental and theoretical model catalyst study, J. Catal. 226 (2004) 88–100.

[12] D. Göbke, Y. Romanyshyn, S. Guimond, J.M. Sturm, H. Kuhlenbeck, J. Döbler, U. Reinhardt, M.V. Ganduglia-Pirovano, J. Sauer, H.-J. Freund, Formaldehyde formation on vanadium oxide surfaces $V_2O_3(0001)$ and $V_2O_5(001)$: how does the stable methoxy intermediate form?, Angew Chem. Int. Ed. 48 (2009) 3695–3698.

[13] B. Beck, M. Harth, N.G. Hamilton, C. Carrero, J.J. Uhlrich, A. Trunschke, S. Shaikhutdinov, H. Schubert, H.-J. Freund, R. Schlögl, J. Sauer, R. Schomäcker, Partial oxidation of ethanol on vanadia catalysts on supporting oxides with different redox properties compared to propane, J. Catal. 296 (2012) 120–131.

[14] Z. Feng, J. Lu, H. Feng, P.C. Stair, J.W. Elam, M.J. Bedzyk, Catalysts transform while molecules react: an atomic-scale view, J. Phys. Chem. Lett. 4 (2013) 285–291.

[15] T. Kropp, J. Paier, J. Sauer, Support effect in oxide catalysis: methanol oxidation on vanadia/ceria, J. Am. Chem. Soc. 136 (2014) 14616–14625.

[16] Q. Wang, R.J. Madix, Partial oxidation of methanol to formaldehyde on a model supported monolayer vanadia catalyst: vanadia on TiO_2, Surf. Sci. 496 (2002) 51–63.

[17] B. Frank, R. Fortrie, C. Hess, R. Schlögl, R. Schomäcker, Reoxidation dynamics of highly dispersed VO_x species supported on γ-alumina, Appl. Catal., A 353 (2009) 288–295.

[18] C.A. Carrero, R. Schloegl, I.E. Wachs, R. Schomaecker, Critical literature review of the kinetics for the oxidative dehydrogenation of propane over well-defined supported vanadium oxide catalysts, ACS Catal. 4 (2014) 3357–3380.

[19] H. Poelman, G. Silversmit, D. Poelman, G.B. Marin, B.S. Sels, Deposition and characterisation of vanadium oxide thin films: Linking single crystal and supported catalyst, Catal. Today 142 (2009) 125–131.

[20] M. Levin, The enhancement of CO hydrogenation on rhodium by TiO_x overlayers, J. Catal. 106 (1987) 401–409.

[21] A.B. Boffa, C. Lin, A.T. Bell, G.A. Somorjai, Lewis acidity as an explanation for oxide promotion of metals: implications of its importance and limits for catalytic reactions, Catal. Lett. 27 (1994) 243–249.

[22] S. Surnev, A. Fortunelli, F.P. Netzer, Structure-property relationship and chemical aspects of oxide-metal hybrid nanostructures, Chem. Rev. 113 (2013) 4314–4372.

[23] J.A. Rodriguez, P. Liu, J. Graciani, S.D. Senanayake, D.C. Grinter, D. Stacchiola, J. Hrbek, J. Fernández-Sanz, Inverse oxide/metal catalysts in fundamental studies and practical applications: a perspective of recent developments, J. Phys. Chem. Lett. 7 (2016) 2627–2639.

[24] J. Zhang, J.W. Medlin, Catalyst design using an inverse strategy: from mechanistic studies on inverted model catalysts to applications of oxide-coated metal nanoparticles, Surf. Sci. Rep. 73 (2018) 117–152.

[25] S.J. Tauster, S.C. Fung, R.L. Garten, Strong metal-support interactions. Group 8 noble metals supported on titanium dioxide, J. Am. Chem. Soc. 100 (1978) 170–175.

[26] S. Kuld, M. Thorhauge, H. Falsig, C.F. Elkjær, S. Helveg, I. Chorkendorff, J. Sehested, Quantifying the promotion of Cu catalysts by ZnO for methanol synthesis, Science (New York, N.Y.) 352 (2016) 969–974.

[27] T. Franz, B. von Boehn, H. Marchetto, B. Borkenhagen, G. Lilienkamp, W. Daum, R. Imbihl, Catalytic CO oxidation on Pt under near ambient pressure: a NAP-LEEM study, Ultramicroscopy 200 (2019) 73–78.

[28] J. Schoiswohl, M. Sock, S. Eck, S. Surnev, M.G. Ramsey, F.P. Netzer, G. Kresse, Atomic-level growth study of vanadium oxide nanostructures on Rh(111), Phys. Rev. B 69 (2004) 1688.

[29] H.H. Rotermund, Imaging of dynamic processes on surfaces by light, Surf. Sci. Rep. 29 (1997) 265–364.

[30] E. Bauer, Low energy electron microscopy, Rep. Prog. Phys. 57 (1994) 895–938.

[31] E. Bauer, Surface Microscopy with Low Energy Electrons, Springer, New York, New York, NY, 2014.

[32] Perdew, Burke, Ernzerhof, Generalized gradient approximation made simple, Phys. Rev. Lett. 77 (1996) 3865–3868.

[33] Blöchl, Projector augmented-wave method, Phys. Rev. B 50 (1994) 17953–17979.

[34] G. Kresse, D. Joubert, From ultrasoft pseudopotentials to the projector augmented-wave method, Phys. Rev. B 59 (1999) 1758–1775.

[35] H.J. Monkhorst, J.D. Pack, Special points for Brillouin-zone integrations, Phys. Rev. B 13 (1976) 5188–5192.

[36] Blöchl, Jepsen, Andersen, Improved tetrahedron method for Brillouin-zone integrations, Phys. Rev. B 49 (1994) 16223–16233.

[37] S. Grimme, Semiempirical GGA-type density functional constructed with a long-range dispersion correction, J. Comput. Chem. 27 (2006) 1787–1799.

[38] T. Kerber, M. Sierka, J. Sauer, Application of semiempirical long-range dispersion corrections to periodic systems in density functional theory, J. Comput. Chem. 29 (2008) 2088–2097.

[39] K. Reuter, M. Scheffler, Composition, structure, and stability of RuO$_2$(110) as a function of oxygen pressure, Phys. Rev. B 65 (2001) 1038.

[40] H. Hellmann (Ed.), Hans Hellmann: Einführung in die Quantenchemie, first ed., Springer Spektrum, Berlin, 2015.

[41] R.P. Feynman, Forces in molecules, Phys. Rev. 56 (1939) 340–343.

[42] J. Schoiswohl, G. Kresse, S. Surnev, M. Sock, M.G. Ramsey, F.P. Netzer, Planar vanadium oxide clusters: two-dimensional evaporation and diffusion on Rh (111), Phys. Rev. Lett. 92 (2004) 206103.

[43] J. Schoiswohl, S. Surnev, M. Sock, S. Eck, M.G. Ramsey, F.P. Netzer, G. Kresse, Reduction of vanadium-oxide monolayer structures, Phys. Rev. B 71 (2005) 165437.

[44] J. Schoiswohl, S. Surnev, F.P. Netzer, G. Kresse, Vanadium oxide nanostructures: from zero- to three-dimensional, J. Phys. Condens. Matter 18 (2006) R1–R14.

[45] M. Hesse, B. von Boehn, A. Locatelli, A. Sala, T.O. Menteş, R. Imbihl, Island ripening via a polymerization-depolymerization mechanism, Phys. Rev. Lett. 115 (2015) 136102.

[46] B. von Boehn, A. Preiss, R. Imbihl, Dynamics of ultrathin V-oxide layers on Rh (111) in catalytic oxidation of ammonia and CO, Phys. Chem. Chem. Phys. 18 (2016) 19713–19721.

[47] Y. de Decker, A. Raghamy, R. Imbihl, Modeling the formation and propagation of VO$_x$ islands on Rh(111) under reactive conditions, J. Phys. Chem. C 123 (2019) 11602–11610.

[48] P.A. Thiel, J.T. Yates, W.H. Weinberg, The interaction of oxygen with the Rh (111) surface, Surf. Sci. 82 (1979) 22–44.

[49] K.A. Peterlinz, S.J. Sibener, Absorption, adsorption, and desorption studies of the oxygen/Rh(111) system using O$_2$, NO, and NO$_2$, J. Phys. Chem. 99 (1995) 2817–2825.

[50] A.S. Mikhailov, Foundations of Synergetics I: Distributed Active Systems, Springer, Berlin, Heidelberg, 1994.

[51] A.S. Mikhailov, A.Y. Loskutov, Foundations of Synergetics II: Complex Patterns, Springer, Berlin, Heidelberg, 1991.

[52] S.S. Mann, T. Seto, C.J. Barnes, D.A. King, Coverage dependence of surface diffusion of hydrogen and deuterium on Rh{111} by laser induced thermal desorption, Surf. Sci. 261 (1992) 155–163.

[53] J. Barth, Transport of adsorbates at metal surfaces: from thermal migration to hot precursors, Surf. Sci. Rep. 40 (2000) 75–149.

[54] Wintterlin, Schuster, Ertl, Existence of a 'Hot' atom mechanism for the dissociation of O$_2$ on Pt(111), Phys. Rev. Lett. 77 (1996) 123–126.

[55] M. Mavrikakis, J. Rempel, J. Greeley, L.B. Hansen, J.K. Nørskov, Atomic and molecular adsorption on Rh(111), J. Chem. Phys. 117 (2002) 6737–6744.

[56] I. Píš, T. Skála, M. Cabala, F. Šutara, J. Libra, M. Škoda, V. Matolín, V. Nehasil, Structural, electronic and adsorption properties of V-Rh(111) subsurface alloy, J. Alloys Compd. 543 (2012) 189–196.

[57] B. von Boehn, R. Imbihl, Chemical wave patterns and oxide redistribution during methanol oxidation on a V-oxide promoted Rh(110) surface, J. Phys. Chem. C 122 (2018) 12694–12703.

[58] B. von Boehn, T.O. Menteş, A. Locatelli, A. Sala, R. Imbihl, Reactive phase separation during methanol oxidation on a V-oxide-promoted Rh(110) surface, J. Phys. Chem. C 122 (2018) 10482–10488.

[59] R. Imbihl, G. Ertl, Oscillatory kinetics in heterogeneous catalysis, Chem. Rev. 95 (1995) 697–733.

[60] H.H. Rotermund, G. Haas, R.U. Franz, R.M. Tromp, G. Ertl, Imaging pattern formation in surface reactions from ultrahigh vacuum up to atmospheric pressures, Science 270 (1995) 608–610.

[61] Z. Sobalik, Structure of monolayer vanadia γ-alumina catalysts as revealed by IR spectra of probe molecules, J. Catal. 127 (1991) 665–674.

[62] A.W. Stobbe-Kreemers, M. Soede, M. Makkee, J.J.F. Scholten, Performance of γ-alumina-supported Wacker catalysts in the oxidation of 1-butene, Appl. Catal., A 131 (1995) 367–381.

[63] M. Ek, Q.M. Ramasse, L. Arnarson, P. Georg Moses, S. Helveg, Visualizing atomic-scale redox dynamics in vanadium oxide-based catalysts, Nat. Commun. 8 (2017) 305.

[64] A. Vittadini, M. Casarin, M. Sambi, A. Selloni, First-principles studies of vanadia-titania catalysts: beyond the monolayer, J. Phys. Chem. B 109 (2005) 21766–21771.